Dynamic analysis of nonlinear behaviour in inertial actuators

M Dal Borgo[1], **M Ghandchi Tehrani**[1] **and S J Elliott**[1]

[1] Institute of Sound and Vibration Research, University of Southampton, University Road, Southampton SO17 1BJ, United Kingdom

E-mail address: mdb2g15@soton.ac.uk

Abstract. Inertial actuators are devices typically used to generate the control force on a vibrating structure. Generally, an inertial actuator comprises a proof-mass suspended in a magnetic field. The inertial force due to the moving mass is used to produce the secondary force needed to control the vibration of the primary structure. Inertial actuators can show nonlinear behaviour, such as stroke saturation when driven at high input voltages. If the input voltage is beyond their limit, they can hit the end stop of the actuator casing and saturate. In this paper, the force generated by an inertial actuator is measured experimentally and numerical simulations of a linear piecewise stiffness model are carried out and compared with the results of analytical methods. First, a numerical model for a symmetric bilinear stiffness is derived and a parametric study is carried out to investigate the change of the end stop stiffness. In addition, the variation of the amplitude of the excitation is considered and a comparison is made with the analytical solution using the harmonic balance method. Finally, experimental measurements are carried out and the results are compared with simulated data to establish the accuracy of the model.

1. Introduction

Research and engineering development are moving onto lightweight, flexible and smart mechatronic structures which are required to perform multiple tasks such as reducing unwanted vibrations, shape morphing, adaptability to varying environmental conditions and structural health monitoring. The nature of these structures such as low weight and high flexibility lead them to operate in an environment where their dynamic behaviour cannot be neglected [1]. As a result, these structures are susceptible to large amplitudes of vibration. The use of passive vibration control typically adds mass to the structures, while the constraints are low weight and flexibility. Hence the use of active control devices such as Active Damping Devices (ADDs) have been used to control vibrations using inertial actuators [2, 3].

The purpose of the ADDs is to add a certain quantity of viscous damping into the structure in order to reduce its level of vibration in particular in the regions of its resonances. ADDs are non-intrusive because they can be attached to an existing structure without any structural modifications, they do not need an external mechanical connection hence the static behaviour of the structure does not change, and they have a wide frequency bandwidth of operation so they can reduce the vibration at several modes of the structure [4], moreover they are suitable for lightweight, flexible structures due to their relatively large force-to-weight ratio [5].

An ADD consists of an inertial (or proof-mass) actuator attached to the structure, a collocated sensor of vibrations (usually an accelerometer) and a controller which feeds back the velocity of the structure to the inertial actuator. The aim of the inertial actuator is to provide an external control force to the structure for the purpose of vibration reduction. The way the proof-mass actuator operates is to use an

input voltage signal to generate (by means of an electromagnetic transducer) the control force on the structure and reacting against a proof-mass, which starts to accelerate [3, 6].

In practical applications, the displacement that the proof-mass can reach is subjected to the stroke length between the end-stops or the dimensions of the actuator casing. For high input voltages, the proof-mass will hit one of the end-stops, hence saturates in the displacement and imparts large shock to the structure [7]. This phenomenon is undesirable in terms of the stability of the closed loop control system, because it can reduce the stability margin. In particular, Baumann *et al.* [8] modelled a proof-mass actuator, which behaves as a linear single degree of freedom (SDOF) system for displacements of the proof-mass lower than the stroke length, and the spring stiffness becomes very large when stroke saturation occurs. They have shown that the instability is due to the fact that the velocity of the structure and the impulse force are in phase when stroke saturation happens, hence it reduces the overall damping of the system. Recently, Wilmshurst *et al.* [9] has conducted an experimental investigation on a stroke saturating inertial actuator, measured its blocked force and estimated the parameters for a bilinear asymmetrical model of the restoring force of the actuator in order to simulate the response of the system and compare the simulated force signals with the experimental data.

In this study, a theoretical model of a stroke saturating inertial actuator with a symmetrical linear piecewise model of the restoring force is assumed. The blocked force of the actuator is then calculated with both analytical and numerical methods when it is driven by a step sine input voltage and the results are presented in the form of time histories and first-order frequency response function (FRF). A comparison with experimental measurements is also carried out. Section 2 covers the dynamic behaviour of a stroke saturated inertial actuator with the numerical simulations, parametric studies, and the comparison between the numerical and the analytical solutions. Section 3 outlines the experimental tests, while conclusions and suggestions for future work are summarized in section 4.

2. Dynamic behaviour of inertial actuators

An inertial actuator is a control device used to generate the secondary force on a structure to minimize its vibration level. This type of actuator is named inertial or proof-mass actuator because of the way it creates a force by reacting against an inertial mass. Its main components are a magnetic proof-mass, a fixed coil and a suspension, which connects the proof-mass with the actuator casing. Its operating principle is to convert electrical power into mechanical power exploiting the Lorentz force law for a current passing through a coil exposed to a uniform magnetic flux [3].

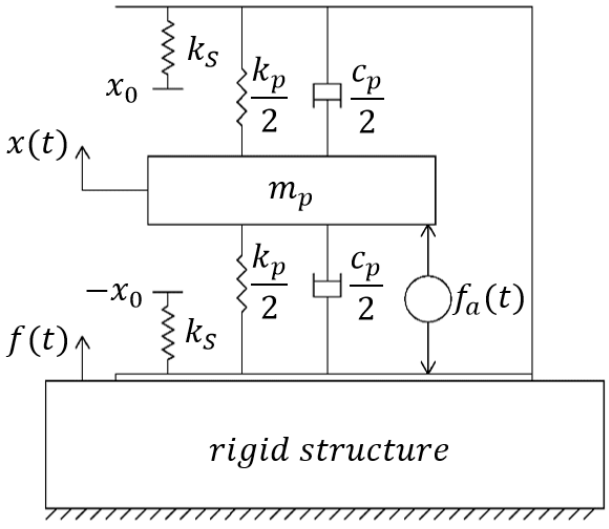

Figure 1. A scheme of an inertial actuator with stroke limit. Stroke saturation makes the stiffness nonlinear.

One limitation for an inertial actuator is that, for practical applications, the stroke length of the proof-mass is finite. This is a problem when there is a need to control low-frequency vibrations, which require a very long stroke length. If the stroke length is exceeded an impact occurs between the proof-mass and the actuator casing, creating a destabilizing control force to the structure [7]. In order to understand the dynamic behavior of an inertial actuator accounting for stroke saturation, a model is created using a lumped parameter system as shown in Figure 1. Referring to Figure 1, the dynamics of the proof-mass actuator can be defined as a SDOF oscillator plus a force generator acting between the inertial mass and the actuator casing. The equation of motion for this model is given as:

$$m_p\ddot{x}(t) + c_p\dot{x}(t) + f_S(x) = f_a(t) \tag{1}$$

where m_p is the proof-mass of the inertial actuator, c_p is the linear damping parameter associated with the proof-mass suspension and $f_a(t)$ is the electromagnetic force generator, which applies equal forces (equal in modules but opposite in directions) onto the proof-mass and the actuator casing and hence to the structure. $x(t)$ denotes the displacement of the proof-mass, while $f_S(x)$ represents the nonlinear restoring force of the system, since the stiffness varies depending on the value of the displacement $x(t)$. In this study, the stroke saturation phenomenon has been modeled as an elastic collision between the proof-mass and the actuator casing in both directions, assuming an equilibrium position of the proof-mass centered between the two end-stops. In this way the model can be seen as a linear SDOF system for displacements lower than the stroke length, and as a nonlinear system with a stiffness added to the model, while stroke saturation occurs. In Figure 1, the impact stiffness k_S can be found from,

$$k_S = k_{NL} - k_p \tag{2}$$

where k_p is the linear stiffness parameter associated with the proof-mass suspension and k_{NL} the stiffness of the overall model for displacements which exceed the stroke length. Referring to Figure 1, the equation of motion for the stroke saturated system can be written, for example for positive displacement above the stroke length x_0 as,

$$m_p\ddot{x}(t) + c_p\dot{x}(t) + k_{NL}(x(t) - x_0) + k_p x_0 = f_a(t) \text{ for } x > x_0 \tag{3}$$

where the term $k_p x_0$ is due to the restoring force until stroke saturation occur and $k_{NL}(x(t) - x_0)$ is the elastic force during the impact between the proof-mass and the end stop. In general, the restoring force for such a model can be written as:

$$f_S(x) = \begin{cases} k_{NL}(x - x_0) + k_p x_0, & x > x_0 \\ k_p x, & |x| \le x_0 \\ k_{NL}(x + x_0) - k_p x_0, & x < -x_0 \end{cases} \tag{4}$$

The values of k_{NL} are shown in relation to the value of the suspension stiffness k_p as follow,

$$k_{NL} = \alpha k_p \tag{5}$$

where α is a multiplying coefficient. Before moving onto the nonlinear behavior of the inertial actuator, the dynamics of the underlying linear system is investigated. Equation (4) is also represented in Figure 2 for several values of the impact stiffness, taking into account equation (5), so the nonlinearity has been modeled as a symmetric piecewise linear stiffness.

Combining equations (1) and (4) for the case of $|x| < x_0$, and taking the Laplace transform with initial conditions set to zero leads to:

$$\left[m_p s^2 + c_p s + k_p\right] X(s) = F_a(s) \tag{6}$$

The transfer function between the displacement of the proof-mass and the generator force is:

$$\frac{X(s)}{F_a(s)} = \frac{1}{m_p s^2 + c_p s + k_p} = \frac{1}{m_p(s^2 + 2\zeta_p\omega_p s + \omega_p^2)} \tag{7}$$

where $\omega_p = \sqrt{\frac{k_p}{m_p}}$ and $\zeta_p = \frac{c_p}{2\sqrt{k_p m_p}}$ are the natural frequency and the damping ratio of the system respectively.

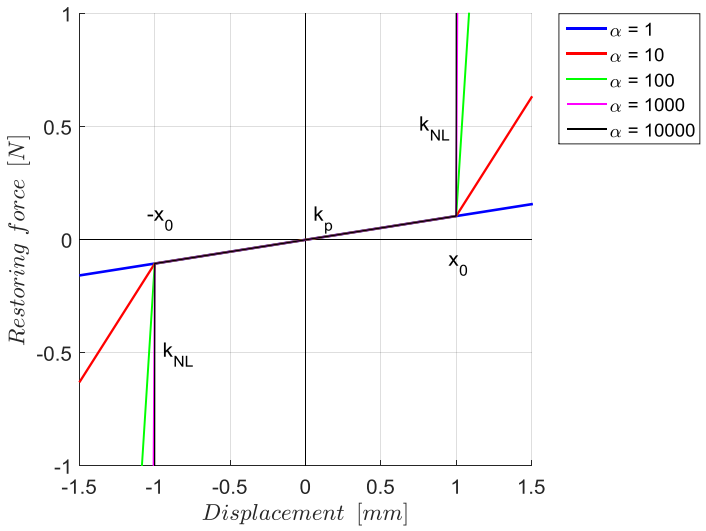

Figure 2. Restoring force for several values of the impact stiffness, from the linear case (large blue line) to strong nonlinear case (thin black line).

To determine the inherent dynamic behavior of the inertial actuator, a rigid and nonmoving supporting structure is attached to the actuator base hence the dynamics of such supporting structure can be ignored. The blocked force imparted by the actuator to the structure can be calculated for different values of the input voltage from the force generator. The total applied force to the structure, the blocked force $f(t)$, can be expressed as:

$$f(t) = c_p\dot{x}(t) + f_S(t) - f_a(t) = -m_p\ddot{x}(t) \tag{8}$$

Taking the Laplace transform yields:

$$F(s) = -s^2 m_p X(s) \tag{9}$$

The equation governing the force generator can be taken for simplicity as:

$$f_a(t) = gv(t) \tag{10}$$

where $v(t)$ is the input voltage and g is a gain term that is determined by the product of the electromagnetic gain of the proof-mass actuator's coil (in N/A) and a power amplifier gain (in A/V). The power amplifier gain has been included in g in order to simplify the comparison between simulated and measured data. Taking into account equations (7), (9) and the Laplace transform of equation (10), the transfer function between the blocked force of the inertial actuator and the input voltage signal can be written as,

$$\frac{F(s)}{V(s)} = \frac{F(s)}{X(s)}\frac{X(s)}{F_a(s)}\frac{F_a(s)}{V(s)} = -g\frac{s^2}{s^2 + i2\zeta_p\omega_p s - \omega_p^2} \tag{11}$$

Assuming a harmonic excitation, hence substituting $s = i\omega$ in equation (11), leads to the frequency response function (FRF) between the blocked force and the input voltage,

$$\frac{F(i\omega)}{V(i\omega)} = g\frac{(\frac{\omega}{\omega_p})^2}{1 + i2\zeta_p\frac{\omega}{\omega_p} - (\frac{\omega}{\omega_p})^2} \tag{12}$$

The FRF magnitude and phase plots for the system described by the parameters given in Table 1 is shown in Figure 3.

Table 1. Lumped parameters of the actuator obtained from the Micromega Dynamics Catalogue [4] and from [9].

Parameter	$m_p\ [kg]$	$c_p\ [Ns/m]$	$k_p\ [N/m]$	$g\ [N/V]$	$x_0\ [mm]$
Value	0.032	1.36	105	0.3	1

It should be noted that for frequencies above the natural frequency of the proof-mass actuator, the blocked force tends to be equal to the output of the force generator that is g times the input voltage signal. For example the blocked force is $0.3\ N$ for this particular actuator, when the input voltage $V_0 = 1V$.

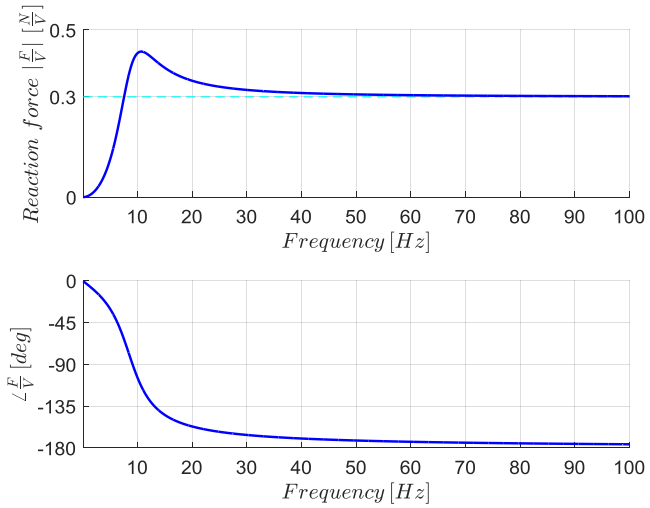

Figure 3. Theoretical FRF (magnitude and phase) between the force $F(i\omega)$ and the voltage $V(i\omega)$ using equation (12).

If the inertial actuator is driven by a large input voltage, stroke saturation may occur, and its behaviour becomes nonlinear and cannot be described by equation (12) since the response depends on the amplitude of excitation. It is however possible to construct FRFs for nonlinear systems using other methods such as harmonic balance method. The important thing is to define the type of input excitation because a nonlinear system responds to them in different ways (i.e. different FRFs). In this study a stepped sinusoidal excitation is chosen. The approach used in this study to approximate the FRF of the nonlinear model of the proof-mass actuator is the harmonic balance method [10]. The aim of this method is to assume that the response is sinusoidal at the same frequency of the input excitation. The equation of motion (1) is linearized and in particular the restoring force (4) is written as,

$$f_S(x) \simeq K_{eq}x \tag{13}$$

where K_{eq} is an equivalent stiffness for a given operating condition. With this approximation a first-order FRF for the linearized system between the input phase-shifted excitation $f_a(t) = F_a\sin(\omega t - \phi)$ and the trial solution $x(t) = Xsin(\omega t)$ can be obtained,

$$\frac{X(i\omega)}{F_a(i\omega)} = \frac{1}{K_{eq} - m\omega^2 + ic\omega} = \Lambda(\omega, X) \tag{14}$$

where $\Lambda(\omega, X)$ denotes the first-order FRF of the nonlinear system, which is amplitude dependent. Expanding a Fourier series equation, for the trial solution $x(t) = Xsin(\omega t)$, considering only the fundamental terms and noting that the restoring force is an odd function (as widely explained in [10]), results in,

$$K_{eq} = \frac{b_1}{X} = \frac{1}{\pi X}\int_0^{2\pi} d\theta\ f_S(X\sin(\theta))\sin(\theta) \tag{15}$$

where b_1 is the fundamental sine term of the Fourier transform and ωt has been replaced by:

$$\theta = \omega t \tag{16}$$

It should be noticed that the integrand of equation (15) changes two times during one cycle of oscillation if $|Xsin(\omega t)|$ exceeds x_0. This can be substituted by an angle $\theta_0 = \omega t_0$ during the cycle, where:

$$\theta_0 = \sin^{-1}\left(\frac{x_0}{X}\right) \tag{17}$$

Than for $\theta = \pi - \theta_0$ the integrand switches back. This happens for the first half cycle and due to the symmetry of the restoring force, the same switching happens for the second half of the cycle. Equation (15) can thus be rewritten as:

$$K_{eq} = k_p + \frac{(k_{NL} - k_p)}{\pi}\left[\int_{\theta_0}^{\pi-\theta_0} d\theta\ \sin(\theta)\left(\sin(\theta) - \frac{x_0}{X}\right) + \int_{\pi+\theta_0}^{2\pi-\theta_0} d\theta\ \sin(\theta)\left(\sin(\theta) + \frac{x_0}{X}\right)\right] \tag{18}$$

hence K_{eq} is the mean value of the stiffness experienced by the system over one cycle. Simplifying equation (18) a final form for K_{eq} is achieved, which is:

$$K_{eq} = k_p\left\{1 + \frac{(\alpha - 1)}{\pi}\left[\pi - 2\sin^{-1}\left(\frac{x_0}{X}\right) - 2\frac{x_0}{X^2}\sqrt{X^2 - x_0^2}\right]\right\} \tag{19}$$

K_{eq} is the describing function, which depends on the amplitude of the response X. The change of the resonant frequency of the nonlinear system with X can be obtained from equation (19). The non-dimensional parameter β is considered as,

$$\beta^2 = \frac{\omega_{res,NL}^2}{\omega_p^2} = \frac{K_{eq}}{k_p} \tag{20}$$

An easier interpretation can be established by means of equation (20), which is plotted in Figure 4 for several α. Indeed, as the response amplitude increases until the end-stop of the inertial actuator ($x_0 = 1\ mm$), the system is linear with stiffness k_p and $\beta = 1$. If $|X|$ increases more than x_0 then a hardened stiffness is encountered and β increases with X.

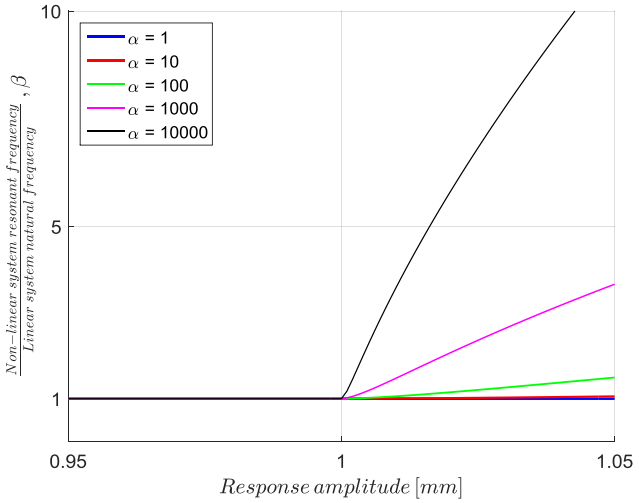

Figure 4. Variation in resonant frequency with excitation level for system with restoring force as in Figure 2.

Combining equation (19) with equation (14), the first-order FRF for the nonlinear system of Figure 1 can be written as:

$$\Lambda(\omega, X) = \frac{1}{k_p\left\{1 + \frac{(\alpha - 1)}{\pi}\left[\pi - 2\sin^{-1}\left(\frac{x_0}{X}\right) - 2\frac{x_0}{X^2}\sqrt{X^2 - x_0^2}\right]\right\} - m_p\omega^2 + ic_p\omega} \tag{21}$$

Implicit equation (21) does not permit to plot the first-order FRF straightly, instead it is rewritten as a homogenous equation, which can be solved by iteration.

In this study the X values of such an equation have been found out using the MatLab nonlinear equation solver *fzero* for given values of the frequency ω and the input force F_a. Then the first-order FRF of the blocked force to the input voltage is derived combining equation (21) with equations (9) and

(10). The resultant FRFs for different values of α are plotted in Figure 8 and compared with those resulting from the method of numerical time integration of equation of motion, which is a common solution procedure for nonlinear vibration problems.

The method of numerical integration of equation of motion gives a time domain solution for the response of the system excited by a stepped sine excitation that must be post-processed with an expansion in terms of Fourier series to obtain the first-order FRF. In an orderly manner, the second order equation of motion (1) is written in state-form as follow:

$$\dot{\mathbf{x}} = \mathbf{A}\mathbf{x} + \mathbf{B}f_a \tag{22}$$

where **x** is the state vector which contains the state variables, **A** is the state matrix and **B** the input vector. Accordingly to equations (1), (4) and (22) the state-space formulation can be entirely written as follow:

$$\begin{Bmatrix} \dot{x}_1 \\ \dot{x}_2 \end{Bmatrix} = \begin{bmatrix} 0 & 1 \\ -\dfrac{k}{m_p} & -\dfrac{c_p}{m_p} \end{bmatrix} \begin{Bmatrix} x_1 \\ x_2 \end{Bmatrix} + \begin{bmatrix} 0 \\ \dfrac{1}{m_p} \end{bmatrix} gv(t) + \begin{bmatrix} 0 \\ \dfrac{(k-k_p)}{m_p} \end{bmatrix} x_0 \text{sign}(x_1(t)) \tag{23}$$

where the stiffness k is given by:

$$\begin{cases} k = k_p \ , & |x| \le x_0 \\ k = k_{NL}, & elsewhere \end{cases} \tag{24}$$

The state-space equation has been solved by numerical integration using the MatLab function *ode45* with fixed time steps over a period of 800 seconds and a sample rate of 20 kHz. Every ten seconds an increasing step applies to the sine excitation frequency. The time history of the blocked force is given by differentiating the solution of the numerical integration for the velocity of the system and consequently applying equation (8) to the calculated acceleration. Figure 5 and Figure 6 show the time histories of the blocked force for the underlying linear system and the nonlinear system respectively.

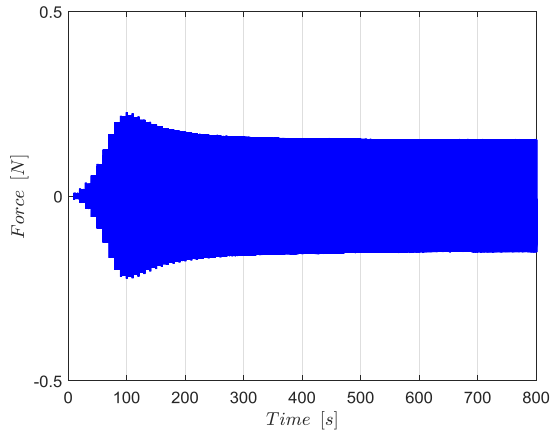

Figure 5. Time history of the blocked force simulated for a stepped sine input signal, increasing of 1 Hz every 10 seconds, for the underlying linear system.

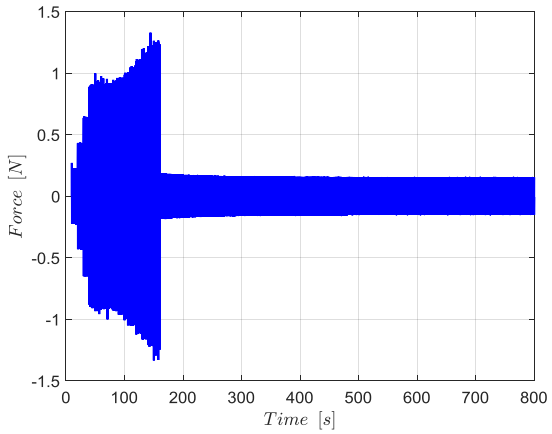

Figure 6. Time history of the blocked force simulated for a stepped sine input signal, increasing of 1 Hz every 10 seconds, for the nonlinear system.

In Figure 5 the behavior of the inertial actuator is linear, so the maximum force is reached at the resonant peak and then the output force is constant for higher values of the frequency. Figure 6 shows a different behavior for the firsts 150 seconds due to the importance of the nonlinear effects at low frequencies. In this case stroke-saturation phenomenon occurs resulting in higher values of the blocked force when compared with the values of the linear case.

(a) 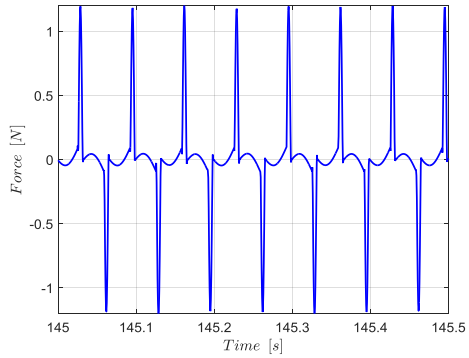

(b) 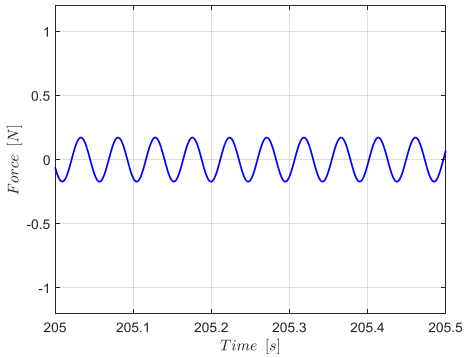

Figure 7. Waveforms of the simulated blocked force: (a) the input signal frequency is $14\ Hz$; (b) the input signal frequency is $20\ Hz$.

The impulses due to the impact between the proof-mass and the end-stops are shown in Figure 7(a). Every peak corresponds to the proof-mass colliding with the actuator casing and then rapidly increasing the blocked force. For higher frequencies the proof-mass does not saturate and there is no distortion in the waveform, as it is shown in Figure 7(b).

The previous simulation has been repeated with a longer signal for every frequency step (50 seconds) and every transient has been removed for the steady-state responses. The first-order FRF in this case is obtained by applying the Fourier series to the blocked force steady-state signal:

$$f(t) = \frac{a_0}{2} + \sum_{n=1}^{\infty}\left[a_n \cos\left(\frac{2\pi n t}{T_p}\right) + b_n \sin\left(\frac{2\pi n t}{T_p}\right)\right] \tag{25}$$

Considering only the fundamental terms a_1 and b_1, which are given by:

$$a_1 = \frac{2}{T_p}\int_0^{T_p} dt\, f(t)\cos\left(\frac{2\pi t}{T_p}\right) \quad \text{and} \quad b_1 = \frac{2}{T_p}\int_0^{T_p} dt\, f(t)\sin\left(\frac{2\pi t}{T_p}\right) \tag{26}$$

The magnitude and phase of the first-order FRF are easily obtained considering the following relationships:

$$M_1 = \sqrt{a_1^2 + b_1^2} \quad \text{and} \quad \phi_1 = \tan^{-1}\left(-\frac{b_1}{a_1}\right) \tag{27}$$

where M_1 represents the magnitude of the response at the fundamental frequency and ϕ_1 is the phase shift at the same frequency. The effect of α on the response of the actuator is investigated and the results are given in Figure 8 in terms of first-order FRFs. Figure 8 shows also a comparison between the harmonic balance method and the numerical integration of equation of motion. The increase of α leads to an increase of the resonant frequency for a given value of the input excitation, as stated in Figure 4. The increase of α also affects the magnitude of the peak of the first-order FRF. In particular the amplitude of the peak decreases when the value of the impact stiffness becomes larger. From Figure 8 for $\alpha \neq 1$ there is a jump of the magnitude in the FRF from high to low value. This happens both in magnitude and phase. Comparing the results given by harmonic balance method and those of numerical integration of equation of motion, there is very good agreement in the magnitude and phase of the FRF for lower values of α while for high values of the impact stiffness the method of the harmonic balance gives a lower resonant frequency and a lower value of the magnitude of the resonant peak.

The nonlinear behaviour of an inertial actuator for a given value of the impact stiffness and increasing values of the input voltage can be clearly seen in Figure 9 from numerical integration. The magnitude and phase of the FRF of the blocked force to the input voltage for several values of the amplitude of the excitation is shown. For small values of the input voltage, less than $0.3\ V$, the system behaves as the underlying linear system of Figure 3, hence all the FRFs are obtained from the linear system. If the input voltage is increased more than $0.3\ V$, both magnitude and phase of the FRF show nonlinear behaviour. This is due to the nonlinearity of the stroke saturation phenomenon. Indeed, an increasing of the input voltage results in an increasing of the resonant frequency of the nonlinear system, which can also be seen in Figure 4 for a given α and an increasing response amplitude. Moreover, the resonant peaks

appear to increase in magnitude with the increase of V_0. There is an explanation to this. If V_0 is larger, the time which the system experiences stroke saturation is larger hence the mean value of the stiffness during one cycle becomes larger. Since the damping of the system is assumed to be always the same, it results that the damping ratio is lower for larger input voltages. The consequence is an higher resonant peak.

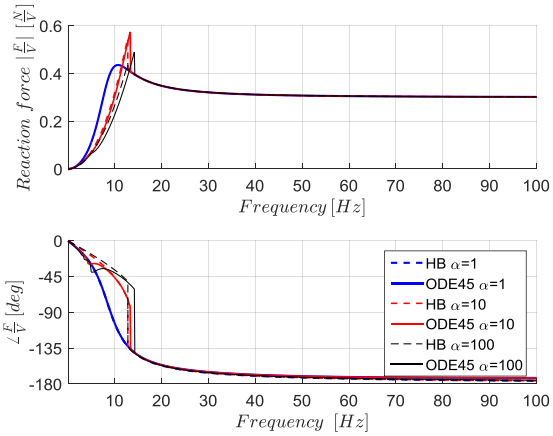

Figure 8. Comparison between first-order FRFs obtained using numerical integration of state-space (23) (solid lines) and harmonic balance method (dashed lines) for $V_0 = 0.5\,V$ and different values of α.

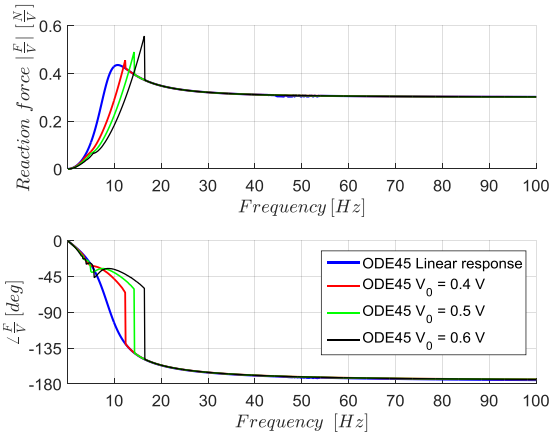

Figure 9. First-order FRFs using numerical integration of the state-space (23) for a given value of the impact stiffness ($\alpha = 100$) and several values of the input voltage amplitude V_0.

Figure 9 also shows that for the first-order FRFs of the nonlinear system the blocked force after the resonant peak drops down suddenly both in magnitude and phase compared to the linear system FRF curve. This kind of behaviour also seen in the time domain response of Figure 6 and Figure 11, later on, for the experimental measurements, is called jump phenomenon. After the frequency of the jump, the stroke saturation does not occour and the system behaves as the underlying linear system.

3. Experimental tests

Experimental measurements of the blocked force of an inertial actuator have been carried out using the following experimental setup, which is also shown in Figure 10. A Micromega Dynamics IA-01 inertial actuator (see [4]) is fixed at his base with a PCB Piezotronics 208C01 ICP force sensor, which is attached to a rigid clamped mass via wax (due to the small entire mass of the actuator and force sensor). The small value of the suspension stiffness of the proof-mass actuator required a horizontal positioning of such actuator in order to avoid the proof-mass ending to one end-stop in static conditions. The input signal is generated by dSpace 1103 through the ControlDesk Next Generation software and they are used also for data acquisition. The dSpace generated signal is amplified by a Micromega Dynamics Rack-04-45N which is connected then with the proof-mass actuator. The measured signal by the force cell is conditioned by a PCB Piezotronics 480E09 ICP sensor signal conditioner prior to entering a dSpace channel.

Figure 11 shows a time history of the recorded signal of the blocked force where the actuator is excited by a stepped sine input voltage starting from $1\,Hz$ and increasing of $0.1\,Hz$ every 5 seconds until $20\,Hz$ and then increasing of $1\,Hz$ until $100\,Hz$, using a sampling rate of $20\,kHz$ and maintaining a constant amplitude of the input excitation V_0. First the actuator is driven with low input voltages, under $0.3\,V$ and an approximately linear behaviour is obtained, which is similar to that of Figure 5 for the simulated time history. Then V_0 is increased to $0.5\,V$ in order to record the output signal while stroke saturation is occurring. In order to obtain the correct information from the input and output signal in terms of time histories, relative amplitudes and phase shifts, the dynamics of the instrumentations used are measured. All the instrumentations are used within the frequency and amplitude range reported in

the data sheets, hence their dynamics are assumed to be linear and time-invariant. The measurements of the FRFs of the power amplifier has been already done by *Wilmshurst et al.* [9] where they indicate a constant $11\ dB$ gain across the frequency range. The measurements on the signal conditioner and analogic/digital converter indicate a gain and a phase shift, which can be neglected in this frequency range. Finally the sensitivity of the force transducer, which is $112.410\ mV/N$ (from the data sheet) is guaranteed to be constant over the frequency range of interest.

Figure 10. A picture of the experimental setup where is possible to distinguish the rigid mass, the force transducer and the inertial actuator placed in horizontal position.

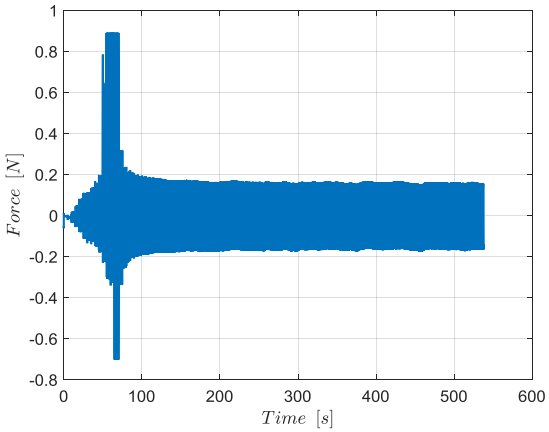

Figure 11. Time history of the blocked force measured for a stepped sine input signal increasing of $1\ Hz$ every 5 seconds.

The measured blocked force time history shown in Figure 11 has an importance to understand the nonlinear behaviour of the inertial actuator due to stroke saturation. Indeed at a certain time, which corresponds to a certain frequency, spikes start to appear as a result of the impact force between the proof-mass and the actuator casing. This phenomenon can be also clearly seen in Figure 12(a) for an input frequency of $12\ Hz$.

(a)

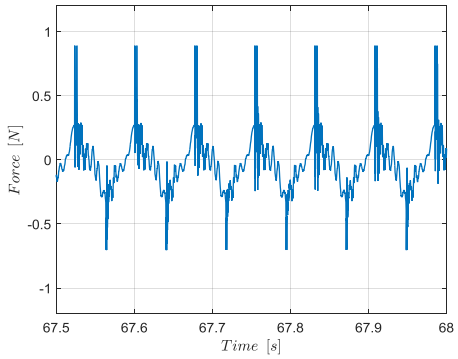

(b)

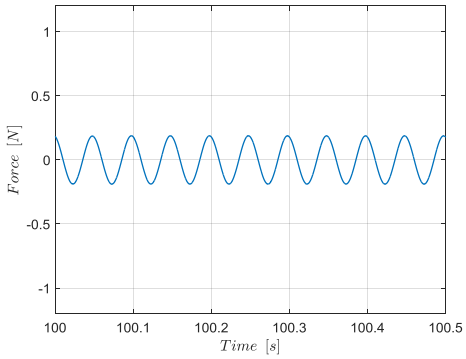

Figure 12. Waveforms of the measured blocked force: (a) the input signal frequency is $12\ Hz$; (b) the input signal frequency is $20\ Hz$.

Over a certain frequency the spikes disappear, as is predicted from the simulations illustrated in Figure 6, resulting in the jump phenomenon. The system then behaves as a linear system and the waveform of the blocked force is sinusoidal, as shown in Figure 12(b). It should also be noticed that the time history of the blocked force is not symmetrical during the stroke saturation phase. In particular, the spikes are only on the upper side of the figure, which implies that the proof-mass saturates only with one end stop and doesn't collide with the other one. This is due to an equilibrium position of the proof-mass that is not centered within the actuator casing. Similar the numerical simulations, the frequency analysis is applied to the blocked force time histories in order to obtain the experimental first-order FRFs

of the blocked force to the input voltage. The coefficients of the fundamental frequency of the Fourier series are taken and combined in order to obtain the magnitude and phase shift, hence using equations (25), (26) and (27). Results are shown in Figure 13 for the underlying linear behaviour and the nonlinear behaviour when the actuator is driven with an input voltage of $0.5\,V$. The experimental FRFs are also compared with those obtained by the simulation using the numerical integration of equation of motion approach.

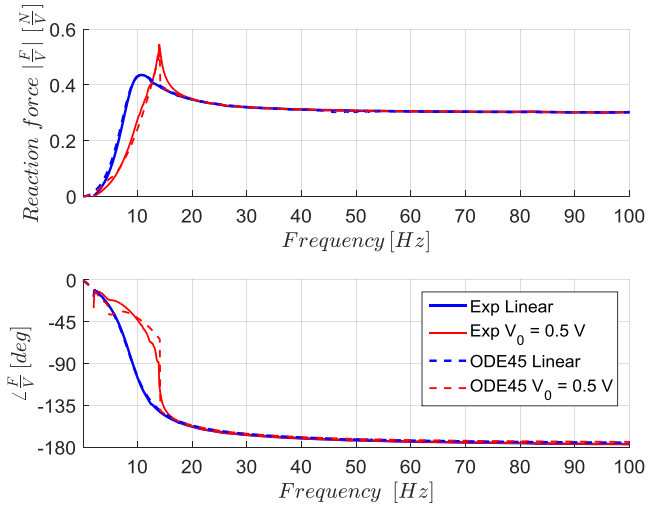

Figure 13. Comparison between FRFs obtained by the experimental data (blue continuous line) and using numerical integration of state-space (23) (red dashed line) with $\alpha = 50$ and $V_0 = 0.5\,V$.

The post-processed experimental data show (in Figure 13) the FRF for the system driven with low input voltages and a first-order FRF for the stroke saturating inertial actuator, which are similar to those obtained for the simulations. In particular there is a very good agreement between the experimental curve and the simulated for low amplitude of the input voltage which is the case of the underlying linear system. For large input voltage, stroke saturation occurs and the resonant peak of the measured FRF is shifted to higher frequency and also the magnitude of the resonant peak is increased. There is a good agreement with the first-order FRF of the simulation for the symmetric piecewise linear model of the inertial actuator and a noticeable discrepancy is due to a less pronounced jump phenomenon in the experimental FRF respect to that predicted with the simulations.

4. Conclusions and further work

An analytical model of a nonlinear proof-mass actuator with a symmetric piecewise linear restoring force was derived using the harmonic balance method in order to obtain the first-order FRF of the blocked force to the input voltage excitation. Also a numerical model in the state-space was derived in order to have an insight into the time history of the output signal for a stepped sine excitation. The first-order FRF was also obtained from the time histories applying the Fourier transform for the fundamental terms. The resulting FRFs of these two different approaches were compared for different values of the impact stiffness and a good agreement between the two for relatively small values of the impact stiffness was achieved. A major difference was in the resonant frequency and magnitude of the resonant peak when the impact stiffness becomes larger. A parametric study was done for the variation of the amplitude of the excitation. Experimental measurements were also carried out and both the time histories of the blocked force and the first-order FRF of the blocked force to the input voltage were compared to the results of numerical simulations. Although the model is a very simple symmetric piecewise linear model, it can describe the nonlinear behaviour fairly well and the results are in good agreement except for the asymmetry in the blocked force time history. Improvements will be made considering the asymmetrical

stiffness and also a more accurate damping model of the impact will be considered as part of the future work.

Acknowledgements
The authors gratefully acknowledge the European Commission for its support of the Marie Curie program through the ITN ANTARES project (General Agreement 606817).

References

[1] Wagg D J and Neild S A 2015 *Nonlinear Vibration with Control - For Flexible and Adaptive Structures (Solid Mechanics and Its Applications)* (Springer)

[2] Fuller C R Elliott S J and Nelson P A 1997 *Active Control of Vibration* (London: Academic Press)

[3] Preumont A 2011 *Vibration Control of Active Structures* (Springer)

[4] Micromega Dynamics [Accessed Jan 2016] *Active Damping Devices and Inertial Actuators* http://www.micromega-dynamics.com/download/category/4-active-damping-device.html

[5] Lindner D K, Zvonar G A and Borojevic D 1994 Performance and control of proof-mass actuators accounting for stroke saturation *AIAA J. Guid. Control Dyn.* **17** pp 1103-08

[6] Zimmerman D C and Inman D J 1990 On the nature of the interaction between structures and proof-mass actuators *J. of Guid. Control Dyn.* **13** pp. 82-88

[7] Chase J G Yim M and Berlin A A 1999 Integrated centering control of inertially actuated systems *Control Eng. Pract.* **7** pp 1079-84

[8] Baumann O N and Elliott S J 2007 Destabilisation of velocity feedback controllers with stroke limited inertial actuators *J. Acoust. Soc. Am.* **121**

[9] Wilmshurst L I Ghandchi Tehrani M and Elliott S J 2013 Nonlinear Vibrations of a Stroke-Saturated Inertial Actuator *11th Int. Conf. in Recent Advances in Structural Dynamics (Pisa)*

Wilmshurst L I 2015 *Analysis and Control of Nonlinear Vibration in Inertial Actuators* PhD thesis Institute of Sound and Vibration Research (University of Southampton)

[10] Worden K and Tomlinson G R 2000 *Nonlinearity in Structural Dynamics: Detection, Identification and Modelling* (CRC Press)